Advances in Geo-Energy Research

Vol. 20, No. 1, p. 85-97, 2026

Original article

Fracture permeability reduction and sealing mechanisms of microbial cementation in underground fractured media: Application to low-permeability reservoirs

Yanlong He[1,2,3], Shizi An[1,4], Tayfun Babadagli[1,5], Keyi Liu[1,3], Lu Bai[1,3], Hai Huang[1,2,3]*

[1]*School of Petroleum Engineering, Xi'an Shiyou University, Xi'an 710065, P. R. China*

[2]*Shaanxi Key Laboratory of Carbon Dioxide Sequestration and Enhanced Oil Recovery, Xi'an 710065, P. R. China*

[3]*Engineering Research Center of Development and Management for Low to Ultra-Low Permeability Oil & Gas Reservoirs in West China, Ministry of Education, Xi'an 710065, P. R. China*

[4]*College of Petroleum Engineering, China University of Petroleum, Beijing 102249, P. R. China*

[5]*Department of Civil and Environmental Engineering, Faculty of Engineering, University of Alberta, Edmonton T6G 1H9, Canada*

Keywords:
Microbial enhanced oil recovery
microbially induced calcium precipitation
indigenous microorganisms
Bacillus megaterium

Cited as:
He, Y., An, S., Babadagli, T., Liu, K., Bai, L., Huang, H. Fracture permeability reduction and sealing mechanisms of microbial cementation in underground fractured media: Application to low-permeability reservoirs. Advances in Geo-Energy Research, 2026, 20(1): 85-97. https://doi.org/10.46690/ager.2026.04.07

Abstract:
Microbially induced calcium precipitation is a promising method for sealing fractures in low-permeability reservoirs, yet the role of anaerobic indigenous microorganisms under reservoir conditions remains unclear. In this study, reservoir samples were anaerobically enriched, and a urease-producing indigenous strain identified as *Bacillus megaterium* was isolated. Its growth, environmental tolerance, stimulation response, biomineralization products, and fracture-sealing performance were systematically evaluated. The strain showed good adaptability to fractured reservoir conditions and produced extracellular polymeric substances that promoted calcium enrichment and calcite formation. Visual fracture experiments demonstrated that microbial cementation significantly reduced fracture permeability and achieved effective sealing. The results further indicate that the dominant sealing mechanism depends on fracture aperture: surface adsorption controls sealing in narrow fractures, whereas particle deposition, settling, and migration become increasingly important in wider fractures. These findings clarify the fracture-sealing mechanisms of indigenous anaerobic microorganisms and support their potential application in subsurface permeability control.

1. Introduction

In recent years, low-permeability reservoirs have become the main focus of oil and gas exploration and development in China (Wang et al., 2017; Hu et al., 2018; Du and Bai, 2024). Such reservoirs are characterized by low matrix permeability, high heterogeneity and complex, varied fracture systems. During water injection, the injected water readily flows along fractures, or the "thief zone", decreasing the utilization efficiency of the injected water (Liu et al., 2019; Li et al., 2024). Thus, it is essential to mitigate reservoir heterogeneity. For decades, polymer gels, microspheres, particles, and biopolymers have been the main sealing agents employed in low-permeability fractured reservoirs (Safdel et al., 2017; Jiang et al., 2024; Zhang et al., 2024). However, traditional sealing agents remain constrained by several drawbacks, including sensitivity to reservoir temperature and water salinity, a potential mismatch between particle size and fracture aperture, the insufficient resistance of some chemical sealing agents, and certain en-

Yandy Scientific Press

*Corresponding author.
E-mail address: stpnet@126.com (Y. He); anshizi1234@163.com (S. An); tayfunbabadagli@hotmail.com (T. Babadagli); 24212010182@stumail.xsyu.edu.cn (K. Liu); 13299197451@163.com (L. Bai); huanghai@xsyu.edu.cn (H. Huang).

Received February 20, 2026; revised March 21, 2026; accepted April 10, 2026; available online April 14, 2026.

vironmental or health risks associated with their application (Wang and Bai, 2018; Chen et al., 2020; Wang et al., 2024; Hu et al., 2025).

Microbial cement based on urea hydrolysis has been studied for various engineering applications, such as ground improvement (Whiffin et al., 2007; Choi et al., 2020), fracture sealing in concrete (Chen et al., 2022), as well as geological CO_2 storage (Lin et al., 2025; Jin et al., 2026). Previous studies addressing fracture sealing have typically poured, sprayed or dripped the treatment solution onto concrete block or immersed fractured samples in the solution (Turner et al., 2023; Zheng et al., 2024). However, profile control for low-permeability reservoirs requires the injection of the treatment fluid into the target location in the reservoir. This shift in application highlights several advantages of microbial cement as a sealing agent, including its low treatment-fluid viscosity, greater durability compared to several conventional chemical agents, adhesive behavior that can strengthen fracture sealing, and compatibility with calcium ions already present in the reservoir water (Minto et al., 2016; Turner et al., 2023).

In terms of microbially induced cementation, previous research has primarily focused on urease-producing aerobic microorganisms, such as *Sporosarcina pasteurii*. For example, Peng and Liu (2019) investigated the effects of temperature on microbial cementation, while Phillips et al. (2018) and Kirkland et al. (2020) used *Sporosarcina pasteurii* in near-wellbore zones of oil reservoirs. However, reports indicate that the microbial cement precipitation induced by *Sporosarcina pasteurii* under anaerobic conditions is negligible (Jain and Arnepalli, 2019). Given that reservoir environments are characterized by high temperature, high pressure, high salinity, and a lack of oxygen, although extensive research has demonstrated the potential of indigenous microorganisms in such conditions for enhanced oil recovery (Sun et al., 2017; Yin et al., 2023), experiments utilizing these microorganisms for microbial cement sealing remain remarkably scarce (He et al., 2025; Liu et al., 2025). This represents a gap in the development of in situ microbial cement-based sealing solutions. Accordingly, one of the main challenges is to harness and utilize urease-producing anaerobic indigenous microorganisms in developing a strategy that addresses reservoir heterogeneity.

In order to reduce fracture permeability and seal fractures in low-permeability media, this study performs laboratory experiments and constructs visualized fracture flow models to investigate the potential of urease-producing anaerobic indigenous microorganisms. It should be noted that *Bacillus megaterium* has been reported as a ureolytic species in previous microbially induced calcium carbonate precipitation (MICP)-related studies, but this has not been verified or mechanistically interpreted from an anaerobic aspect. Therefore, this organism is further investigated here under conditions relevant to low-permeability reservoirs. Specifically, this study aimed to analyze the microbial compositions of original and enriched reservoir samples, identify and optimize the selected strain under reservoir relevant conditions, characterize microbial cement growth and products, and evaluate fracture sealing and permeability reduction using visualized fracture models.

2. Materials and methods

2.1 Strain screening and characterization

Drilling cuttings were obtained from the Yanchang Formation of the Wuqi Oilfield in northern Shaanxi. The microorganism screening method was similar to that reported by Minto et al. (2016). To facilitate the enrichment and screening of urease-producing microorganisms, the urea medium utilized contained 5 g/L NaCl, 20 g/L urea, 2 g/L glucose, and 2 g/L peptone (see the Supporting Material, Method. S0). For more detailed information on the composition and specific method of the culture medium, refer to Supporting Material Method S1 for the screening of microorganisms. Subsequently, the selected strains were sequenced by Shanghai Pysenno Biotechnology Co., Ltd.

The growth characteristics of microorganisms are an important basis for engineering applications. One mL of stimulated strain solution was inoculated into the urea liquid medium and cultured at 47 °C with shaking at 180 r/min. The absorbance method was used to measure microbial concentration (see the Supporting Material, Method. S2). The spectrophotometer was set to 600 nm, and the cuvette had an optical path length of 10 mm. Urease activity, as an important indicator of a microorganism's ability to decompose urea, was assessed using the conductivity method, consistent with established protocols. The urease activity of the strain was determined by measuring the change in solution conductivity during urea hydrolysis over time (Maleki-Kakelar et al., 2022) (See Supplementary file: Urease Activity Determination Method. S3 for specific operation details). The pH of the culture medium was determined using a pH meter, and all experiments were performed in triplicate.

2.2 Environment factors and stimulation medium

Microbial cement production is closely related to urease activity. Therefore, single-factor experiments were conducted to evaluate the effects of environmental factors and stimulation medium components on urease activity (Table 1), while response surface methodology was further applied to optimize the stimulation medium (Table 2). The inoculum size in both the single-factor experiment and the response surface experiment was 1 mL of the 12-h bacterial culture. The primary culture conditions were 47 °C and a pH of 7 for 39 h, and the primary medium was a urea liquid medium. The pH and urease activity were measured using a pH meter (PHS-25, Shanghai INESA Scientific Instrument Co., Ltd.) and a conductivity meter (DDS-307, Shanghai INESA Scientific Instrument Co., Ltd.).

Based on single-factor experiments on the stimulation medium, urease activity (Y_1) and the solution's final pH (Y_2) were used as the response variables. The carbon and nitrogen sources and urea concentration were optimized for urease activity. Taking the Box-Behnken Design principle as a basis, a response surface optimization design with three factors and three levels was adopted (Dong et al., 2022).

Table 1. Single factor design of environmental factors and stimulation medium.

Stimulation medium					Environmental factors			
Carbon	C_c (g/L)	Nitrogen	C_n (g/L)	C_u (g/L)	Temperature (°C)	pH	$C_{Ca^{2+}}$ (g/L)	$C_{Mg^{2+}}$ (g/L)
Glucose	1	Peptone	1	10	17	4.0	11.1	9.52
Maltose	5	Ammonium chloride	5	20	27	5.0	22.2	19.04
Soluble starch	10	Ammonium sulfate	10	30	37	7.0	33.3	28.56
Sucrose	15	/	15	40	47	8.0	44.4	38.08
/	20	/	20	50	57	9.0	55.5	47.61
/	/	/	/	60	67	/	/	/

Notes: C_c, C_n and C_u represent the concentrations of carbon, nitrogen and urea sources, respectively; $C_{Ca^{2+}}$ and $C_{Mg^{2+}}$ represent the concentrations of calcium and magnesium ions.

Table 2. Variables and levels used for the box-behnken design.

Variable	Component	Level of variable (g/L)		
		-1	0	+1
X_1	Sucrose	3	5	7
X_2	Peptone	8	10	12
X_3	Urea	15	20	25

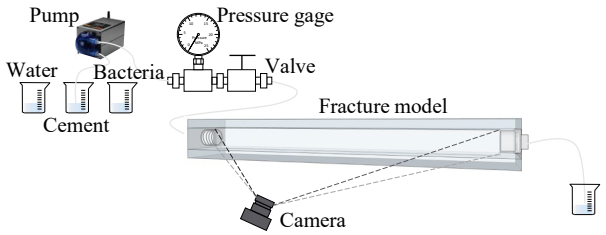

Fig. 1. Schematic diagram of sealing the visual fracture model.

2.3 Characteristics of the microbial cement

2.3.1 Static microstructure characterization

Twenty-five mLs of the stimulation medium were prepared and placed into an anaerobic bottle. The urea-liquid medium was prepared as described in Section 2.1, except that glucose was replaced by sucrose. Next, 1 mL of the stimulated strain solution was added to the culture medium. Subsequently, 25 mL of 22.2 g/L $CaCl_2$ solution was injected to simulate a Ca^{2+}-rich environment. The resulting medium was incubated at 47 °C in a constant-temperature incubator, and microbial cement growth was observed. During cultivation, the medium was withdrawn with a syringe and its pH was measured.

The microbial cement produced in anaerobic bottles was carefully collected. Samples were washed three times with sterile deionized water and dried at 50 °C for 12 h. The crystal structure was analyzed using X-ray diffraction (XRD, D8 ADVANCE, Bruker, Beijing) using a Cu anode (40 kV, 40 mA). Samples were scanned from 5° to 80° (2θ) at 12°/min with a 0.02° step size. Jade 6 software was used for analysis. The microstructure was observed directly with scanning electron microscopy (SEM, MAIA3, TESCAN, Shanghai).

2.3.2 Evaluation of dynamic fracture sealing

(1) Fracture model

MICP was investigated in fractures with varying apertures. For this purpose, fracture flow cells were fabricated using two layers of transparent polycarbonate. The polycarbonate flow cells, measuring 20 cm in length and 5 cm in width, were designed to facilitate the visual monitoring of microbially induced calcite precipitation on fracture surfaces over time. Each flow cell consisted of a smooth top layer, a fractured plate in the center (including a threaded interface), and a lower etched layer (Fig. S1). Fig. 1 illustrates a schematic of the experimental setup. Calcite precipitation was tracked over time using a camera. The fracture flow cells were in the horizontal position in all the experiments presented here, with the digital camera placed on the side of the flow cells.

Natural cores were used to create fractured core models simulating reservoir fractures. First, the natural core was split into two blocks. Then, sealing tape was applied to cover the sides of the two split cores to ensure that the fluid flowed only from the fracture end face. The method for making the fractured cores was similar to that applied by Wang and Bai (2018). The fractured core, first dried and then saturated with water, was placed in a core holder with a confining pressure of 3 MPa. The plunger pump was then opened, and the pressure difference across the core holder inlet and outlet was recorded once the pressure and flow rate stabilized. Permeability was determined using the liquid method, and fracture permeability was calculated using Darcy's formula.

(2) Injection strategy

This study utilized a stage injection method simulating the distribution of the indigenous microbe (Dai et al., 2025). Following the permeability measurement, 5 mL of bacterial suspension (OD_{600} = 2.3-2.6, Fig. S6) was injected, followed by a 60-minute static period to allow the attachment of bacteria to solid surfaces. Next, 20 mL of water was injected to

separate the bacterial suspension and cementing solution to prevent calcite precipitation occurring within the pump and tubing lines, and to simulate the distribution of indigenous microorganisms in the fractures. Afterwards, 1 fracture volume of the cementing solution was injected. The injection rate during the experiment was 0.2 mL/min (Zhang et al., 2024).

Darcy's law was applied to calculate the permeability of fractures before and after bio-cement treatment (Zhang et al., 2024):

$$q = \frac{kA}{\mu}\frac{\Delta P}{L} \tag{1}$$

where q denotes the flow rate, cm^3/s; K denotes the core permeability, D; A represents the cross-sectional, cm^2; μ denotes the dynamic viscosity of the pore fluid, mPa·s; ΔP denotes the pressure difference, 10^{-1} MPa; L is the flow path length, cm. For the reader's convenience, 1 D = 0.987 μm^2.

The fracture sealing efficiency and residual resistance factor was calculated based on fracture permeability before and after *Bacillus megaterium* treatment (Zhang et al., 2024) as follows:

$$\eta = \frac{K_1 - K_2}{K_1} \times 100\% \tag{2}$$

$$\mathrm{RRF} = \frac{K_b}{K_a} \tag{3}$$

where η represents sealing efficiency, K_1 denotes the core permeability before bio-cement treatment, D; and K_2 is the core permeability after bio-cement treatment, D; RRF means residual resistance factor, K_b means core permeability before water flood, D; K_a means core permeability after water flood post treatment, D.

3. Results and discussion

3.1 Basic characteristics of indigenous microorganisms in oil reservoirs

3.1.1 Original and enriched microbial composition

In this investigation, rock cuttings were collected from different layers (Chang4+5, Chang6, Chang8, and Chang9) of the Yanchang Formation in the Yanchang oilfield, Shaanxi Province, China. Microbial communities in the initial and enriched rock cutting samples were analyzed. In the original samples (Fig. 2(a)), *Paludibacter*, *Fontibacter*, *Pseudomonas*, and *Hydrogenophaga* were relatively abundant genera, and their abundances were not significantly different across the sample groups. After clustering the samples using the relative abundance table, the classification units and samples were sorted, and the results are presented in Fig. 2(b). It can be seen that the microbial composition of Chang 8 and Chang 9 samples was relatively similar. *Paludibacter*, *Paracoccus*, *Fangibacter*, *Alishewanella*, *Lysinicrobium*, *Alkaliflexus*, *Geobacter*, *Shewanella*, *Ruminococcus*, UCG-014, and Desulfomonas were more abundant in the Chang 4+5 sample, while Ercella, *Hydrogenophaga* and Anaerocolumna were more abundant in the Chang 6 sample. In the Chang 9 sample, the abundance of Anaerovorax was relatively high, whereas *Pseudomonas*, *Thauera* and Halomonas were more abundant in the Chang 8 sample.

In the enriched samples (Fig. 2(c)), *Bacillus* was the most abundant genus in all four groups. *Acinetobacter* followed, which was mainly found in the Chang 9 sample. Using a relative abundance table, clustering and sorting of taxonomic units and samples yielded a species composition heatmap (Fig. 2(d)). After enrichment and cultivation, samples Chang 4+5 and 8 showed similar compositions, as did Chang 6 and 9. The abundance of *Bacillus* was similar across Chang 4+5, Chang 6, and Chang 8, but lower in Chang 9. In Chang 4+5, the most abundant genera after *Bacillus* were Microbacterium, Aeromonas, *Shewanella*, and *Fibromonas*. In Chang 8, *Rhodococcus*, *Pseudomonas* and *Vibrio* were the next most abundant genera after *Bacillus*. In Chang 9, the order of genera was *Bacillus* followed by *Thauera*, *Clostridium* sensu stricto 3, *Acinetobacter*, and *Lysinibacillus*. In Chang 6, the major genera after *Bacillus* were *Hydrogenophaga*, *Paenarthrobacter*, *Enterococcus*, *Exiguobacterium*, *Alishewanella*, and *Salipaludibacillus*.

In the comparison of composition before and after sample enrichment, *Bacillus* became the most abundant after enrichment. It is the most likely microorganism to produce urease in the reservoir, consistent with the source of urea-decomposing microorganisms reported in the existing research. However, this inference still requires further verification, since the distribution of microorganisms in different strata after enrichment is quite different, and the best approach is to find the most widely distributed microorganisms.

3.1.2 Screening, sequencing and growth of strains

Based on the community changes outlined in Section 3.1.1, urease-producing microorganisms were considered to most likely originate from the genus *Bacillus*. This matches previous findings for strains such as *Sporosarcina pasteurii* and *Bacillus megaterium*. *Bacillus megaterium* and *Sporosarcina pasteurii* are representative urease-producing bacteria (Jongvivatsakul et al., 2019; Tang et al., 2020; Dong et al., 2025). Compared to others, these two species adapt well, have larger surface areas, and produce microbial cement quickly and efficiently (Tang et al., 2020). By comparing the original culture medium with the final culture medium, an indigenous urease-producing anaerobic microorganism was found in the reservoir of the Yanchang Formation (Fig. S2). After genetic sequencing (Fig. S3) and phylogenetic tree construction (Fig. 3(c)), HN-01 was identified as *Bacillus megaterium* (CGMCC NO.24776), consistent with our expectations. However, *Sporosarcina pasteurii*, though widely used, was not detected in the reservoir rock cutting samples, indirectly suggesting that this species does not suit the reservoir environment. Many studies also showed that microbial cement precipitation by *Sporosarcina pasteurii* is negligible under anaerobic conditions (Martin et al., 2012; Jain and Arnepalli, 2019).

The microflora of the indigenous microorganism HN-01 on the urease screening medium (Fig. 3(a)) appeared as smooth, regular edges and opaque dots that were easily picked up. According to Fig. 3(b), HN-01 was observed as a short rod-shaped bacterium measuring approximately 2 μm in length. The 16S rDNA sequences of HN-01 were submit-

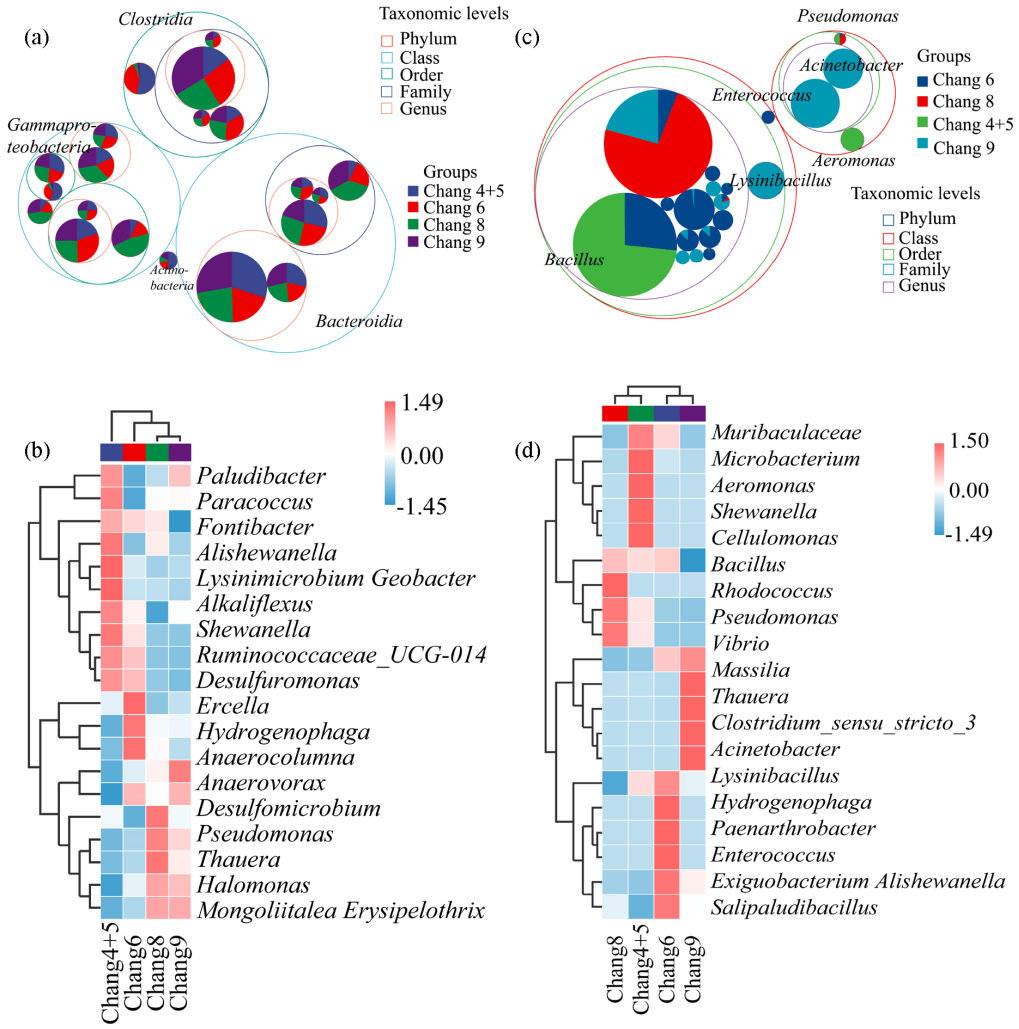

Fig. 2. Sample species composition heatmap and classification grade tree: (a) (c) Classification grade tree of the original and enriched sample and (b) (d) heatmap of the original and enriched sample.

ted to the NCBI database under project accession number SRR15733470. Microbial concentration (OD_{600}) was used to evaluate microbial growth, and urease activity was also considered as a very important indicator. Microbial growth consists of four phases (Fig. 3(d)): Lag phase (0-12 h), exponential growth phase (12-27 h), stationary phase (27-45 h), and decline phase (> 45 h). *Bacillus megaterium* growth was matched with that reported in previous studies (Sun et al., 2019b). Because urease activity and bacterial concentration was to be considered in the experiment, the exponential growth (12-27 h) and the stationary phases (27-45 h) were critical. The pH curve (Fig. 3(e)) remained unchanged or decreased after 45 h, further confirming urease decomposition. The decrease in pH during the lag and exponential growth phases may have been attributed to the microorganism continuously producing acid in the solution. Similar observations were reported by Ferris et al. (2004).

3.2 Environment adaptability and optimization of urease activity

3.2.1 Environmental adaptability

Urease, as a protein biocatalyst, is strongly influenced by environmental factors, among which temperature is a key variable. As shown in Fig. 4(a), urease activity increased with the temperature rising from 17 to 47 °C. Similar trends have been observed by Xie et al. (2023), Sun et al. (2019a), and Jiang et al. (2016). When the temperature exceeded 47 °C, urease activity decreased gradually, indicating that 47 °C was the optimum temperature for urease production. Temperature affects urease in two opposing ways: It accelerates reaction kinetics, whereas excessive heating may also cause protein denaturation. As shown in Fig. 4(a), when the reservoir temperature was lower than the optimal temperature, that is, 17-47 °C, it mainly accelerated the reaction speed; when the temperature was higher than the optimal temperature, that is, 47-57 °C, it mainly inactivated urease, whereas it still had high activity.

Studies have typically placed the optimal pH range for maximum urease activity at 7-9 (Shi et al., 2022; Whiffin et al., 2007). As shown in Fig. 4(b), urease activity remained

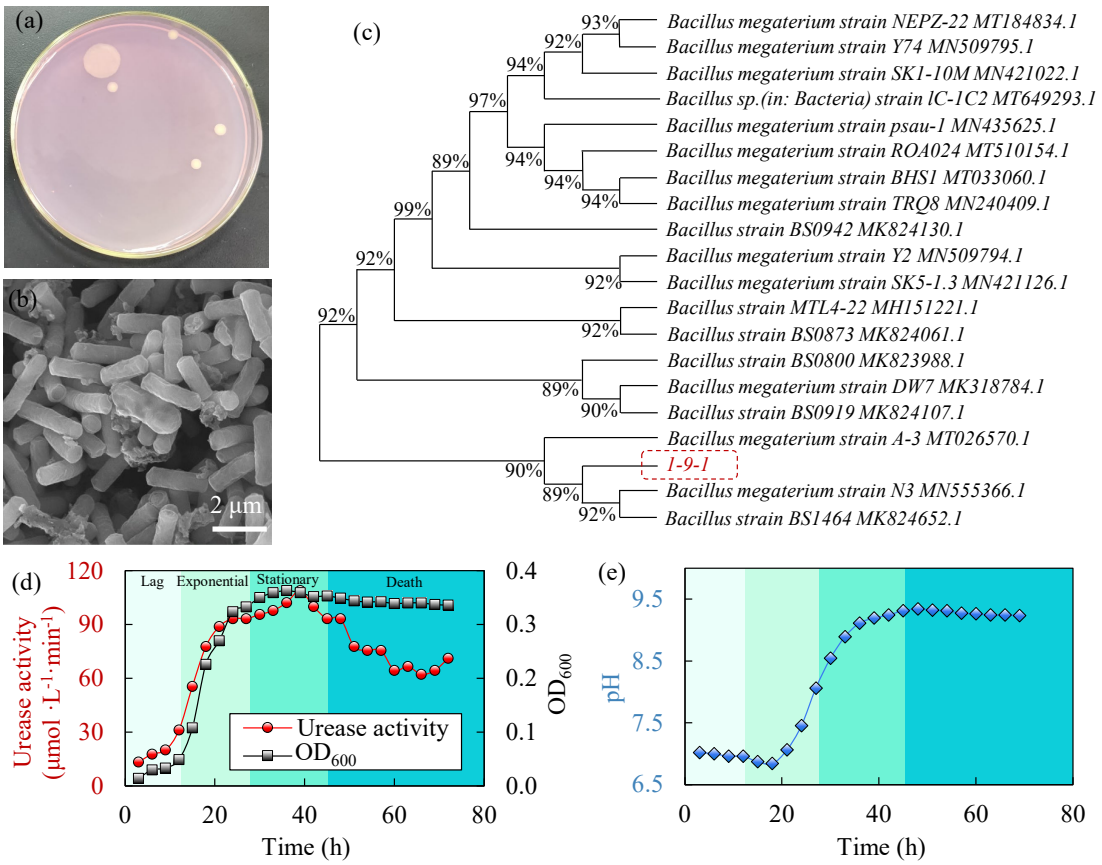

Fig. 3. Indigenous microorganism HN-01: (a) Plate diagram of strain HN-01 (b) SEM image of strain HN-01, (c) phylogenetic tree of strain HN-01, (d) curve of urease activity and strain concentration and (e) pH curve.

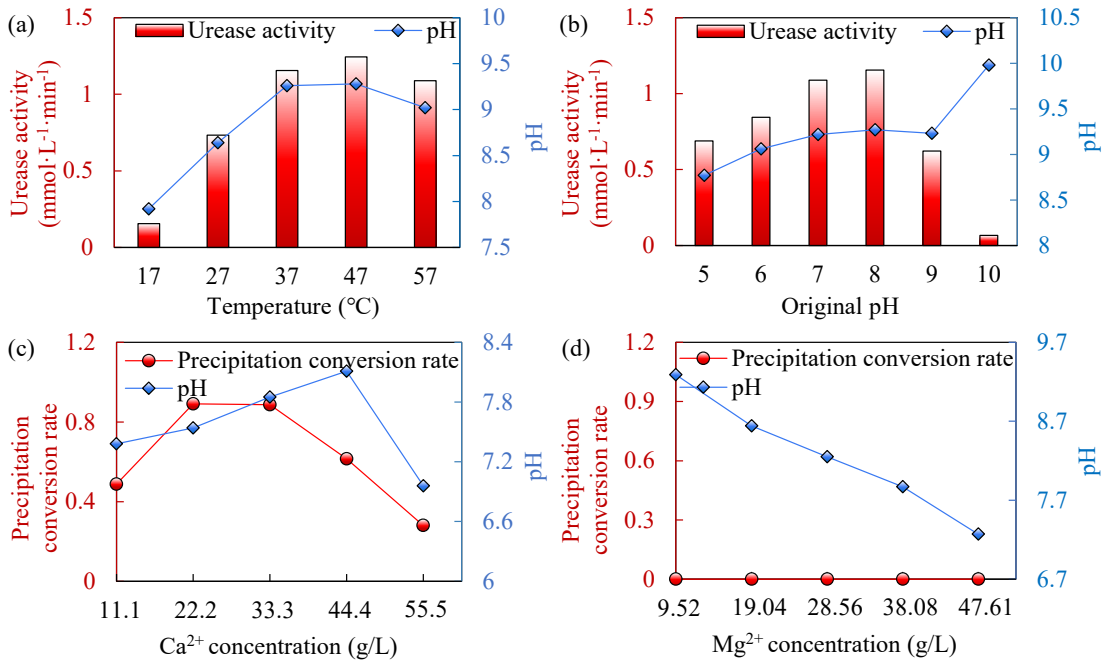

Fig. 4. Results of single-factor optimization experiment: (a)-(d) Optimization of temperature, initial pH, Ca^{2+} concentration, and Mg^{2+} concentration.

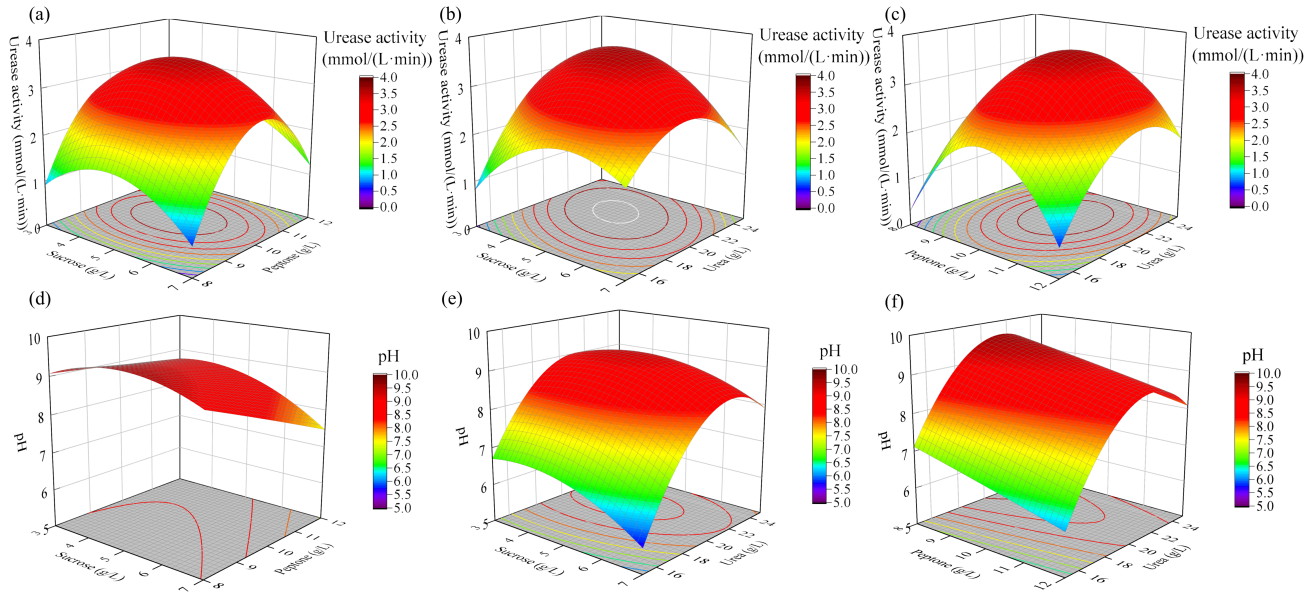

Fig. 5. Results of response surface experiment: (a) (d) Effects of saccharose and peptone on urease activity and pH, (b) (e) effect of saccharose and urea on urease activity and pH and (c) (f) effect of urea and peptone on urease activity and pH.

relatively high when the initial pH ranged from 5 to 9, and the optimum initial pH was 8. This result is consistent with the findings of Sun et al. (2019a) in their study on *Bacillus megaterium*. Fig. 4(b) shows that urease activity decreased sharply at pH 10, which may be because the strong alkalinity affected the cell membrane permeability and cell metabolism. Furthermore, the solution pH influenced not only the three-dimensional enzyme structure but also the ionization states of the enzyme binding and catalytic site. The pH of the medium also had an effect on the separation of substrate and coenzyme, thereby affecting enzyme binding to the substrate (Xie et al., 2023). Accordingly, microbial cement sealing technology can be applied in weakly acidic to weakly alkaline reservoir environments.

Ca^{2+} and Mg^{2+} are important reactants in the production of microbial cement. In situ, urease-producing microorganisms utilize calcium ions in oil reservoirs without any negative effects. In this study, $CaCO_3$ precipitation conversion was higher when the Ca^{2+} concentration was 4.0-16.0 g/L (Fig. 4(c)), whereas the conversion rate decreased at higher Ca^{2+} concentrations. This is consistent with previous reports that excessive Ca^{2+} can inhibit urease activity (Erdmann et al., 2025). The Mg^{2+} concentration did not reach the solubility product of $MgCO_3$, hence no $MgCO_3$ precipitation occurred (Fig. 4(d)). These results provide only a preliminary evaluation under the tested reservoir-relevant factors and are not a full compatibility assessment with actual formation water. Therefore, further testing of Na^+, total salinity and multi-ion coupling using simulated formation brine is recommended.

3.2.2 Stimulation medium

Based on the single-factor experimental results (see Supplementary Material Fig. S4), sucrose was identified as the best carbon source and peptone as the best nitrogen source. To further optimize these findings, a Box-Behnken Design response surface experiment was applied, enabling the refinement of process parameters for optimal urease activity. To clarify the variable interaction, this study employed a square model with coefficients of determination of $R^2_{urease} = 0.9816$ and $R^2_{pH} = 0.9839$. Given that a coefficient of determination (R^2) ranging from 0.94 to 0.99 indicates sufficient model accuracy, the resulting second-order polynomials (4) and (5) were deemed reliable. Furthermore, according to the prediction equation, the optimal medium comprised sucrose (4.622 g/L), peptone (10.196 g/L), and urea (21.419 g/L):

$$\begin{aligned} Y_1 &= 3.53 - 0.1395X_1 + 0.2858X_2 + 0.4435X_3 \\ &\quad - 0.0027X_1X_2 - 0.5967X_1X_3 + 0.1311X_2X_3 \\ &\quad - 0.8173X_1^2 - 1.65X_2^2 - 1.01X_3^2 \\ R^2 &= 0.9816 \end{aligned} \tag{4}$$

$$\begin{aligned} Y_2 &= 9.04 - 0.3387X_1 - 0.4612X_2 + 0.9400X_3 \\ &\quad - 0.29X_1X_2 + 0.1875X_1X_3 + 0.0375X_2X_3 \\ &\quad - 0.4650X_1^2 - 0.0150X_2^2 - 1.46X_3^2 \\ R^2 &= 0.9839 \end{aligned} \tag{5}$$

The results of variance analysis were obtained from the quadratic model (Table S1). The influencing factor was significant when the p value was less than 0.05. Table S1 shows that the two factors with the greatest influence on urease activity were peptone concentration and urea concentration. The peptone and urea concentrations affected the growth of the indigenous microorganism HN-01 and thus influenced urease activity. The most critical factor affecting the solution's pH was urea concentration. This is because urea, an essential participant in MICP, is hydrolyzed by urease to produce ammonia, which inhibits urease activity at high pH values (Sun et al., 2019a; Xie et al., 2023). All three-dimensional diagrams revealing the relevant interactions are shown in Fig. 5. In

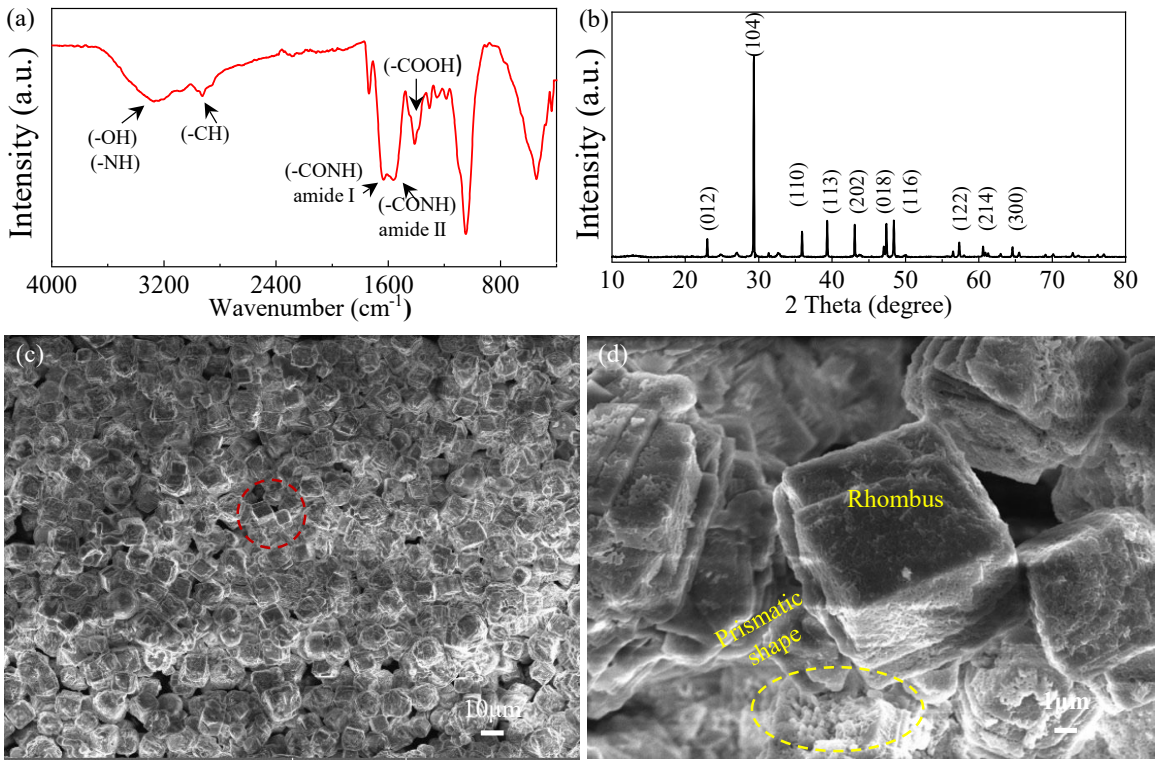

Fig. 6. XRD and SEM analysis of microbial cement: (a) FTIR of extracellular polymer, (b) X-ray diffraction of microbial cement, (c) and (d) 1,000× and 10,000× SEM images of microbial cement in anaerobic bottles.

this study, urease activity was significantly affected by peptone concentration ($p = 0.0158$) and urea concentration ($p = 0.0017$). Moreover, the sucrose concentration ($p = 0.0033$), peptone concentration ($p = 0.0006$), and urea concentration ($p < 0.0001$) had significant effects on pH. Regarding the interactions, X_1X_3 (sucrose concentration and urea concentration, $p = 0.0023$, Fig. 5(b)) significantly affected the urease activity, and X_1X_2 (sucrose concentration and peptone concentration, $p = 0.0330$, Fig. 5(d)) significantly affected the medium pH.

3.3 Characteristic analysis of microbial cement

3.3.1 Static morphological features

The growth of microbial cement in an anaerobic bottle was observed throughout the incubation (see Supplementary Material Fig. S5), which suggested that microbial cement accumulated through both adsorption and deposition. The microbial cement production included three distinct stages: supersaturation of the solution, overcoming of the nucleation energy barrier, and spontaneous growth of crystals on the stable nucleus. Previous studies have shown that calcite may precipitate in both bacteria-containing and bacteria-free systems (Mitchell et al., 2010). Because HN-01 is a Gram-positive strain, negatively charged groups exposed on the cell surface may lower the nucleation barrier and favor Ca^{2+} enrichment (Mountassir et al., 2014). The FTIR results further showed that the extracellular polymeric substances (EPS) secreted by HN-01 contained $-OH$ and $-COOH$ functional groups. Combined with the findings of previous studies, these groups may participate in Ca^{2+} binding and provide potential nucleation sites during biomineralization. However, because EPS yield, zeta potential and Ca^{2+} binding capacity were not quantified in this study, EPS is interpreted here as a participating factor rather than a dominant one in nucleation.

In the MICP/enzyme induced calcium precipitation system, reported microbial cement commonly occurs in the forms of calcite, vaterite and aragonite (Al Imran et al., 2018; Almajed et al., 2019). The XRD results (Fig. 6(b)) showed ten peaks at 23.1°, 29.4°, 36.0°, 39.4°, 43.2°, 47.5°, 48.5°, 57.4°, 60.7°, and 64.7°, which are characteristic of the (012), (104), (110), (113), (202), (018), (116), (122), (214), and (300) planes of calcite, respectively (Standard XRD pattern of calcite, PDF#72-1214). The presence of aragonite and vaterite phases was not observed. No aragonite or vaterite peaks were detected, indicating that calcite was the dominant $CaCO_3$ polymorph under the tested anaerobic culture conditions. Previous studies have shown that bacterial type, EPS, temperature, and solution chemistry may all affect the crystal form (Dhami et al., 2013; Achal and Pan, 2014). In the present study, temperature and EPS may have contributed to the dominance of calcite; however, because no aerobic/anaerobic control experiments or comparative tests under different ionic strengths were conducted, the independent role of anaerobic conditions in polymorph regulation cannot be confirmed.

SEM was employed to examine the microscopic morphology of microbial cement. The reported forms include prismatic, ball and needle morphologies (Lin et al., 2023). Each shape corresponds to a different crystalline form; for example,

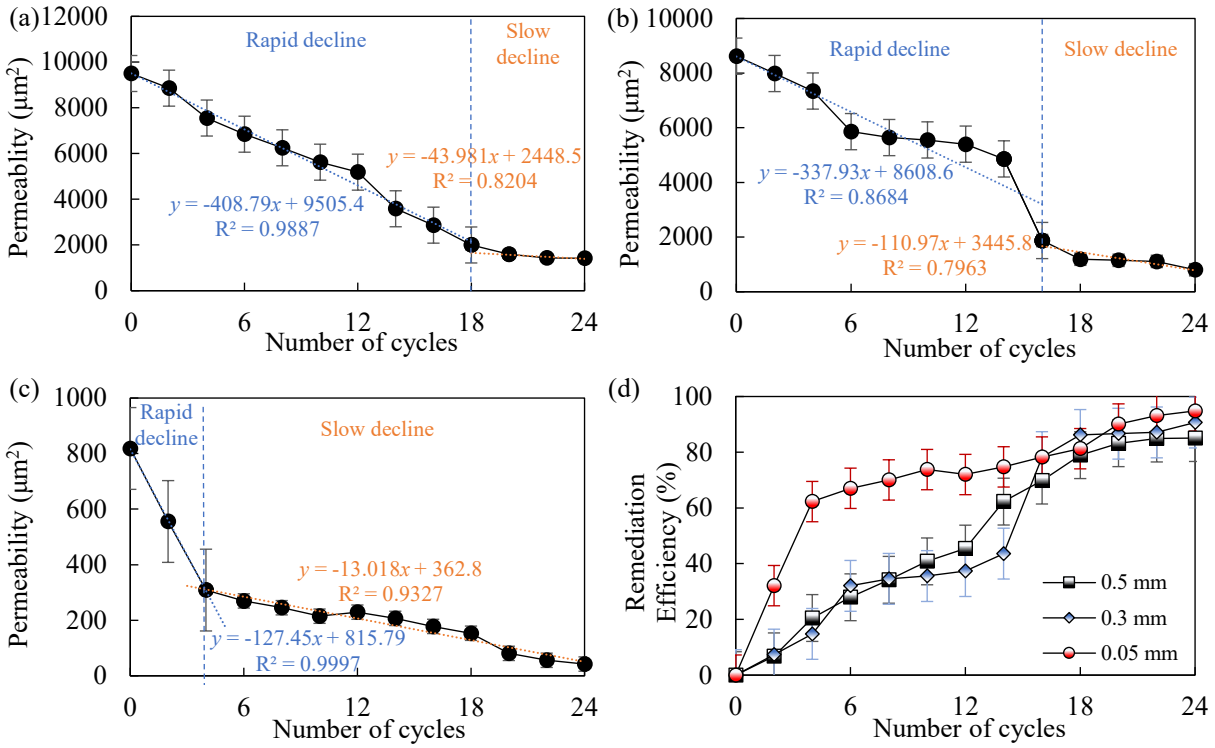

Fig. 7. Effect of microbial cement on fracture sealing: (a)-(c) Permeability changes of 0.5, 0.3, 0.05 mm fracture and (d) sealing efficiency of fractures with different apertures.

prismatic $CaCO_3$ crystals are calcite, spherical crystals are vaterite, and acicular crystals are aragonite. In this study, most microbial cement produced in the anaerobic bottle was rhombus-shaped and prismatic, the side lengths ranged from 5 to 10 μm, and it was mostly calcite. As mentioned earlier, culture temperature and extracellular polymers might have contributed to calcite production.

3.3.2 Dynamic fracture sealing and permeability reduction

(1) Permeability change

The fracture sealing efficiency for different apertures is shown in Fig. 7. With an increasing number of injection cycles, fracture permeability decreased, leading to a gradual increase in the fracture sealing effect. Among the tested apertures, the 0.05 mm fracture exhibited the highest sealing efficiency, followed by the 0.3 mm fracture, and lastly the 0.5 mm fracture. This trend occurred because sealing a large aperture fracture requires more microbial cement (Shi et al., 2024). Furthermore, Fig. S7 illustrates that the macroscopic distribution of microbial cement varied notably across fractures with different apertures:

1) In the 0.5 mm fracture, microbial cement was mainly deposited at the bottom of the fracture and less microbial cement was adsorbed on the fracture surface. The amount of microbial cement near the outlet was greater than that near the inlet, indicating evident migration before deposition. The fracture permeability decreased from 9,500 to 1,416.667 μm^2, with a reduction of 85.09%. After the 20th injection cycle, the decline rate of fracture permeability decreased. After fitting the permeability data, the slope of the fitting curve decreased from 408.79 to 43.981.
2) In the 0.3 mm fracture, microbial cement occurred as deposition and adsorption onto surfaces. More microbial cement was retained on the fracture surface and bottom, and the spatial distribution was relatively uniform. The permeability decreased from 8,621.201 to 805 μm^2, with a decrease of 90.66%. After the 16th injection cycle, the decline rate of fracture permeability slowed down, and the slope of the data fitting curve decreased from 337.93 to 110.97.
3) In the 0.05 mm fracture, microbial cement mainly adsorbed on the fracture surface and was distributed relatively uniformly. The permeability decreased from 818.45 to 42.301 μm^2, with a reduction of 94.83%. After the fourth cycle, the decline rate of fracture permeability slowed down, and the slope of the permeability fitting curve decreased from 127.45 to 13.018.

Based on the permeability data before and after treatment, the RRF was further calculated to preliminarily characterize the residual flow resistance effect of the microbial plugging system. The RRF values of the 0.5, 0.3, and 0.05 mm fractures were 6.71, 10.71, and 19.35, respectively. These results indicate that microbial cementation not only reduced fracture permeability significantly but also generated an increasingly stronger residual resistance effect as the fracture aperture decreased. In particular, the highest RRF obtained in the 0.05 mm fracture suggests that the microbial cement system was

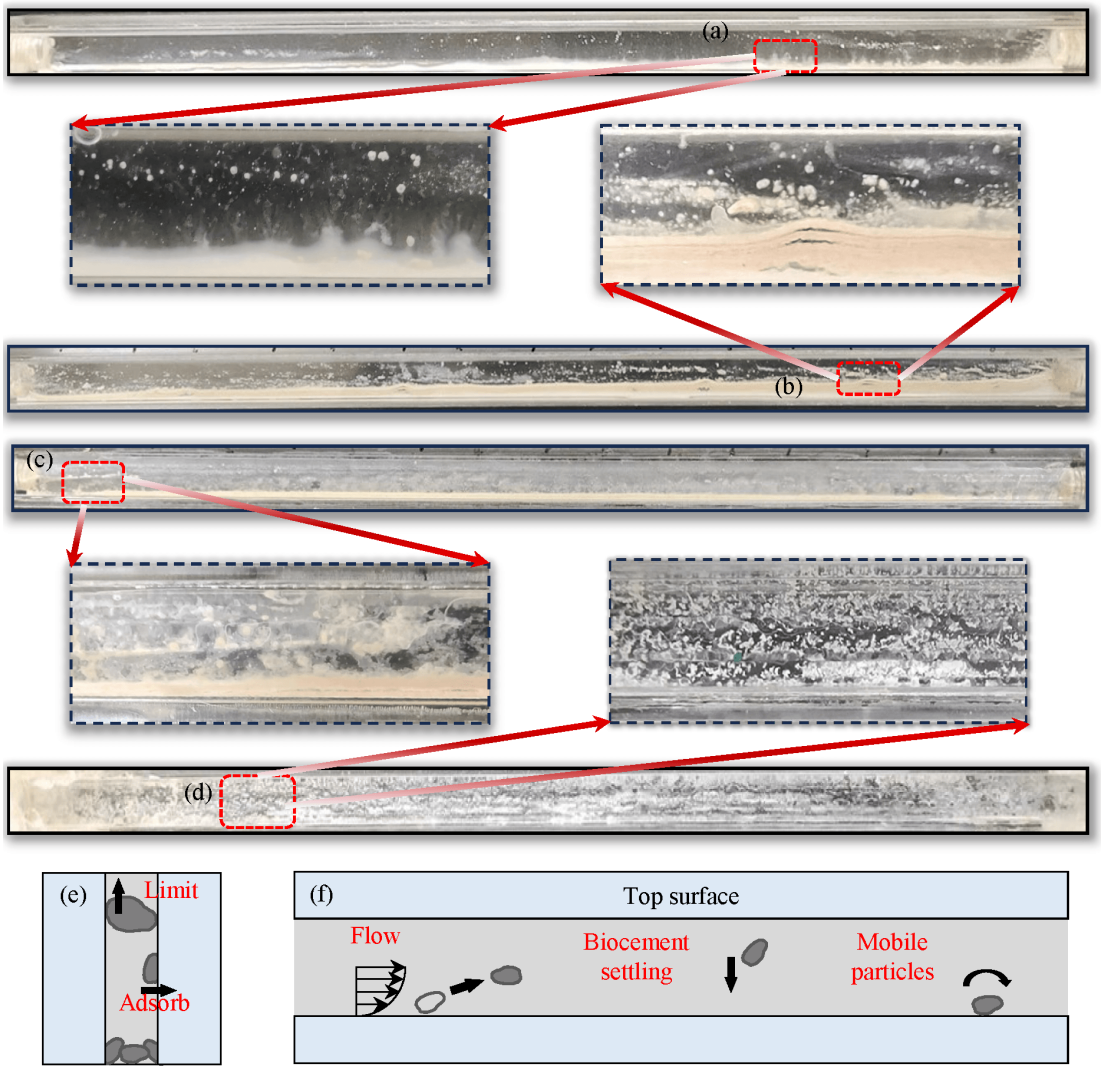

Fig. 8. Growth effect of microbial cement in the fracture model: (a) Extracellular polymers in the fracture, (b)-(d) distribution of microbial cement within 0.5, 0.3 and 0.05 mm fracture and (e)-(f) distribution of microbial cement in fracture side and front view.

more effective in restricting subsequent fluid flow in relatively narrow fractures.

It should be noted that the transparent fracture model was primarily used to visualize the deposition and adsorption behavior of biomineralization products within fractures, and it was not intended to fully reproduce the seepage conditions of actual low-permeability reservoirs. To improve reservoir relevance, an additional 0.3 mm fractured-core displacement experiment was included. The results showed a marked decline in permeability after treatment, indicating that this method can also achieve substantial permeability reduction and sealing under flow conditions closer to those in porous media. The fractured core sealing performance is shown in the Supporting Material (Fig. S8). Nevertheless, verification under confining pressure, in situ stress, and real formation-water conditions should be performed.

The decline rate of single fracture permeability slowed down because microorganisms' adsorption sites filled the entire fracture at the initial stage of sealing. However, with the extended injection cycle, microbial cement gradually occupied the fracture space, mainly through adsorption and deposition (Fig. S7). The injection volume of cement fluid decreased, and the decline rate of permeability gradually slowed down. The spatial distribution observed here differs somewhat from reports by Mountassir et al. (2014), Wu et al. (2019) and Minto et al. (2016). One possible reason is that the staged heterogeneous injection strategy used in this study better mimics indigenous microbial distribution, reduces the risk of severe inlet clogging, and enhances more uniform in-fracture retention.

(2) Multi-scale fracture sealing mechanism

Observing the sealing process of the visual fracture model revealed that flocculent material appeared before microbial cement formation. This behavior is consistent with the static experimental results, as the extracellular polymer disappeared after 30 minutes as mineralization progressed (Figs. 8(a) and 8(b)). According to the distribution of microbial cement in the visual fracture model (Fig. S7), microbial cement mainly

seals fractures by precipitation and adsorption. In the 0.5 mm fracture, the deposited microbial cement formed layered accumulations because the larger aperture allowed greater migration and settling, and fracture flow still dominated after treatment, even though permeability was reduced by 85.09%. By contrast, in the 0.05 mm fracture, microbial cement was mainly adsorbed on the fracture surface, converting channel-dominated flow into pore-like flow, thereby significantly reducing permeability (Liu et al., 2024).

Thus, based on the evolution of permeability and its spatial distribution, this study proposes a mechanism for anaerobic indigenous microbial sealing in fractures in low-permeability reservoirs. In large-aperture fractures, settling velocity, shear velocity and spatial migration become more important, and surface adsorption contributes to initial retention, whereas in intermediate apertures, adsorption and deposition jointly control the final sealing pattern. The spatial distribution of microbial cement is governed by settling velocity, shear velocity, fracture aperture, and surface adsorption (Figs. 8(e) and 8(f)). Given these findings, this study offers laboratory-scale mechanistic interpretation and trends, while quantitative relationships for the adsorption amount, deposition rate, and critical fracture aperture remain to be established in future work.

4. Conclusions

In this study, a urease-producing strain was isolated from reservoir environments and its stimulation medium and environmental adaptability were optimized through single-factor experiments and response surface methodology. By integrating microbial community analysis, with biomineral characterization and visualized fracture experiments, a laboratory-scale framework for fracture sealing and permeability reduction by anaerobic indigenous microorganisms was established.

The results indicated that *Bacillus* became the dominant genus in the reservoir environment after enrichment; strain HN-01 entered the logarithmic growth phase within 12 h. FTIR, XRD and SEM analyses indicated that HN-01 secreted EPS containing $-OH$ and $-COOH$ functional groups, and produced predominantly calcite under the tested anaerobic conditions. In dynamic fracture experiments, microbial cement reduced the permeability by more than 80%. Moreover, the calculated residual resistance factors were 6.71, 10.71 and 19.35 for the 0.5, 0.3 and 0.05 mm fractures, respectively. Based on permeability evolution and visualized spatial distribution, the existence of an adsorption-deposition competition is proposed: Adsorption dominates in narrow fractures, whereas settling and spatial migration become more significant in large fractures, and the two mechanisms jointly operate in intermediate apertures. This reveals the dominant role of fracture aperture in controlling microbial cement distribution and therefore provides a theoretical basis for the targeted sealing of fractures with different apertures. At the same time, it must be noted that this study remains a laboratory-scale investigation. Further work should evaluate the effects of confining pressure, real formation water, and multi-ion coupling, as well as explore the composite cementation behavior of HN-01 with other microorganisms or treatment strategies.

Acknowledgements

This work was supported by the National Natural Science Foundation of China (Nos. 52474040 and 52474043), the Shaanxi Province Key Research and Development Plan (No. 2024GX-YBXM-496), and the Shaanxi Key Laboratory of Carbon Dioxide Sequestration and Enhanced Oil Recovery (No. YJSYZX25SKF0010).

Supplementary file

https://doi.org/10.46690/ager.2026.04.07

Conflicts of interest

The authors declare no competing interest.

References

Achal, V., Pan, X. Influence of calcium sources on microbially induced calcium carbonate precipitation by *Bacillus* sp. CR2. Applied Biochemistry and Biotechnology, 2014, 173: 307-317.

Al Imran, M., Shinmura, M., Nakashima, K., et al. Effects of various factors on carbonate particle growth using ureolytic bacteria. Materials Transactions, 2018, 59(9): 1520-1527.

Almajed, A., Tirkolaei, H. K., Kavazanjian Jr, E., et al. Enzyme induced biocementated sand with high strength at low carbonate content. Scientific Reports, 2019, 9(1): 1135.

Chen, X., Li, Y., Liu, Z., et al. Investigation on matching relationship and plugging mechanism of self-adaptive micro-gel (SMG) as a profile control and oil displacement agent. Powder Technology, 2020, 364: 774-784.

Chen, Y., Wang, S., Tong, X., et al. Crystal transformation and self-assembly theory of microbially induced calcium carbonate precipitation. Applied Microbiology and Biotechnology, 2022, 106(10): 3555-3569.

Choi, S., Chang, I., Lee, M., et al. Review on geotechnical engineering properties of sands treated by microbially induced calcium carbonate precipitation (MICP) and biopolymers. Construction and Building Materials, 2020, 246: 118415.

Dai, Q., Pan, X., Tang, C., et al. A bio-healing method for underground long rock fractures with high bridging rate. Journal of Rock Mechanics and Geotechnical Engineering, 2025, 18(2): 1359-1367.

Dhami, N., Reddy, S., and Mukherjee, A. Biomineralization of calcium carbonate polymorphs by the bacterial strains isolated from calcareous sites. Journal of Microbiology and Biotechnology, 2013, 23(5): 707-714.

Dong, H., Zhang, F., Xu, T., et al. Culture-dependent and culture-independent methods reveal microbe-clay mineral interactions by dissimilatory iron-reducing bacteria in an

integral oilfield. Science of The Total Environment, 2022, 840: 156577.

Dong, Z., Pan, X., Tang, C., et al. An adjustable bio-sealing method for rock fracture leakage mitigation. Journal of Rock Mechanics and Geotechnical Engineering, 2025, 17(1): 220-232.

Du, S., Bai, L. Future potential research hotspots on the precise integration of geology and engineering in low-permeability oil reservoirs. Advances in Geo-Energy Research, 2024, 14(1): 4-7.

Erdmann, N., Aldabbousi, K., Strieth, D. Investigating the influential factors on microbially induced calcium carbonate precipitation: Effects of cell density, temperature, and calcium concentration. Discover Applied Sciences, 2025, 7(7): 696.

Ferris, G., Phoenix, V., Fujita, Y., et al. Kinetics of calcite precipitation induced by ureolytic bacteria at 10 to 20 °C in artificial groundwater. Geochimica et Cosmochimica Acta, 2004, 68(8): 1701-1710.

He, Y., Liu, K., Huang, T., et al. Microbial community assembly and functional adaptation of urease-producing bacteria in oil reservoirs: Driven by phase heterogeneity and selective enrichment. Journal of Environmental Chemical Engineering, 2025, 13(6): 120521.

Hu, W., Wei, Y., and Bao, J. Development of the theory and technology for low permeability reservoirs in China. Petroleum Exploration and Development, 2018, 45(4): 646-656.

Hu, Z., Zhang, Y., Wang, J., et al. Experimental study of a circulation agent dynamic plugging for multi-scale natural fractures. Petroleum Science, 2025, 22(9): 3641-3654.

Jain, S., Arnepalli, D. Biochemically induced carbonate precipitation in aerobic and anaerobic environments by *Sporosarcina pasteurii*. Geomicrobiology Journal, 2019, 36(5): 443-451.

Jiang, H., Yang, H., Pan, R., et al. Performance and enhanced oil recovery efficiency of an acid-resistant polymer microspheres of anti-CO_2 channeling in low-permeability reservoirs. Petroleum Science, 2024, 21(4): 2420-2432.

Jiang, N., Yoshioka, H., Yamamoto, K., et al. Ureolytic activities of a urease-producing bacterium and purified urease enzyme in the anoxic condition: Implication for subseafloor sand production control by microbially induced carbonate precipitation (MICP). Ecological Engineering, 2016, 90: 96-104.

Jin, A., Park, E., Li, C., et al. Geological CO_2 storage in heterogeneous saline aquifers: Insights into the mechanisms of thermal and density effects. Advances in Geo-Energy Research, 2026, 19(3): 216-230.

Jongvivatsakul, P., Janprasit, K., Nuaklong, P., et al. Investigation of the crack healing performance in mortar using microbially induced calcium carbonate precipitation (MICP) method. Construction and Building Materials, 2019, 212: 737-744.

Kirkland, C. M., Thane, A., Hiebert, R., et al. Addressing wellbore integrity and thief zone permeability using microbially-induced calcium carbonate precipitation (MICP): A field demonstration. Journal of Petroleum Science and Engineering, 2020, 107060.

Lin, H., Zhou, M., Li, B., et al. Mechanisms, application advances and future perspectives of microbial-induced heavy metal precipitation: A review. International Biodeterioration & Biodegradation, 2023, 178: 105544.

Lin, X., Zheng, X., Wen, Y. et al. Microbial-induced carbon dioxide (CO_2) mineralization: Investigating the biomineralization chemistry process and the potential of storage in sandstone reservoir. Applied Energy, 2025, 377: 124268.

Liu, M., Wang, J., Luo, H., et al. Microstructurally uniform, high-strength bio-cementation via synergistic microbial- and enzyme-induced calcium carbonate precipitation. Chemical Engineering Journal, 2025, 524: 169343.

Liu, Q., Wang, J., Sun, Z., et al. Microbially mediated rock fine fracture mineralization sealing: Evolution of flow channels and the resulting transmissivity reduction. Engineering Geology, 2024, 334: 107525.

Liu, Y., Zou, C., Zhou, D., et al. Novel chemical flooding system based on dispersed particle gel coupling in-depth profile control and high efficient oil displacement. Energy & Fuels, 2019, 33(4): 3123-3132.

Li, N., Zhu, S., Li, Y. et al. Fracturing-flooding technology for low permeability reservoirs: A review. Petroleum, 2024, 10(2): 202-215.

Maleki-Kakelar, M., Aghaeinejad-Meybodi, A., Sanjideh, S. et al. Cost-effective optimization of bacterial urease activity using a hybrid method based on response surface methodology and artificial neural networks. Environmental Processes, 2022, 9(1): 7.

Martin, D., Dodds, K., Ngwenya, B., et al. Inhibition of *Sporosarcina pasteurii* under anoxic conditions: Implications for subsurface carbonate precipitation and remediation via ureolysis. Environmental Science & Technology, 2012, 46(15): 8351-8355.

Minto, J., MacLachlan, E., El Mountassir, G., et al. Rock fracture grouting with microbially induced carbonate precipitation. Water Resources Research, 2016, 52(11): 8827-8844.

Mitchell, A., Dideriksen, K., Spangler, L., et al. Microbially enhanced carbon capture and storage by mineral-trapping and solubility-trapping. Environmental Science & Technology, 2010, 44(13): 5270-5276.

Mountassir, G., Lunn, R., Moir, H., et al. Hydrodynamic coupling in microbially mediated fracture mineralization: Formation of self-organized groundwater flow channels. Water Resources Research, 2014, 50(1): 1-16.

Peng, J., Liu, Z. Influence of temperature on microbially induced calcium carbonate precipitation for soil treatment. PLoS One, 2019, 14(6): e0218396.

Phillips, A., Troyer, E., Hiebert, R., et al. Enhancing wellbore cement integrity with microbially induced calcite precipitation (MICP): A field scale demonstration. Journal of Petroleum Science and Engineering, 2018, 171: 1141-1148.

Safdel, M., Anbaz, M., Daryasafar, A., et al. Microbial enhanced oil recovery, a critical review on worldwide

implemented field trials in different countries. Renewable and Sustainable Energy Reviews, 2017, 74: 159-172.

Shi, L., Yang, X., Zhang, B., et al. Investigation on the permeability reduction of biogrouting process in rock fracture: Influence factor and hydrological variation. Journal of Cleaner Production, 2024, 473: 143571.

Shi, W., Wang, M., Wu, L., et al. Study of concrete crack repair using Bacillus megaterium. Advances in Materials Science and Engineering, 2022, 2022: 6188680.

Sun, S., Luo, Y., Zhou, Y., et al. Application of Bacillus spp. in pilot test of microbial huff and puff to improve heavy oil recovery. Energy & Fuels, 2017, 31(12): 13724-13732.

Sun, X., Miao, L., Tong, T., et al. Study of the effect of temperature on microbially induced carbonate precipitation. Acta Geotechnica, 2019a, 14: 627-638.

Sun, X., Miao, L., Wu, L., et al. Improvement of biocementation at low temperature based on *Bacillus megaterium*. Applied Microbiology and Biotechnology, 2019b, 103(17): 7191-7202.

Tang, C., Yin, L., Jiang, N., et al. Factors affecting the performance of microbial-induced carbonate precipitation (MICP) treated soil: A review. Environmental Earth Sciences, 2020, 79(5): 94.

Turner, R., Castro, G., Minto, J., et al. Treatment of fractured concrete via microbially induced carbonate precipitation: From micro-scale characteristics to macro-scale behaviour. Construction and Building Materials, 2023, 384: 131467.

Wang, L., Tian, Y., Yu, X., et al. Advances in improved/enhanced oil recovery technologies for tight and shale reservoirs. Fuel, 2017, 210: 425-445.

Wang, Y., Wang, Z., Ali, A., et al. Microbial-induced calcium precipitation: Bibliometric analysis, reaction mechanisms, mineralization types, and perspectives. Chemosphere, 2024, 362: 142762.

Wang, Z., Bai, B. Preformed-particle-gel placement and plugging performance in fractures with tips. SPE Journal, 2018, 23(6): 2316-2326.

Whiffin, V., Paassen, L., Harkes, M. Microbial carbonate precipitation as a soil improvement technique. Geomicrobiology Journal, 2007, 24(5): 417-423.

Wu, C., Chu, J., Wu, S., et al. 3D characterization of microbially induced carbonate precipitation in rock fracture and the resulted permeability reduction. Engineering Geology, 2019, 249: 23-30.

Xie, D., Zhang, R., Wang, J. The influence of environmental factors and precipitation precursors on enzyme-induced carbonate precipitation (EICP) process and its application on modification of recycled concrete aggregates. Journal of Cleaner Production, 2023, 395: 136444.

Yin, J., Wei, X., Hu, F., et al. Halotolerant Bacillus velezensis sustainably enhanced oil recovery of low permeability oil reservoirs by producing biosurfactant and modulating the oil microbiome. Chemical Engineering Journal, 2023, 453: 139912.

Zhang, L., Ni, J., Wang, C., et al. Study on plugging the multiscale water channeling in low-permeability heterogeneous porous media based on the growth of bacteria. SPE Journal, 2024, 29(8): 4248-4265.

Zheng, Y., Li, R., Wang, J., et al. Innovative and environmentally friendly MICP surface curing: Enhancing mechanical and durability properties of concrete. Journal of Cleaner Production, 2024, 478: 143962.